RESEARCH ARTICLE

Galvanically Isolated On-Board Charger Fully Integrated With 6-Phase Traction Motor Drives

PAOLO PESCETTO, (Member, IEEE), MATIAS FERNANDO TRONCOSO CRUZ, (Member, IEEE), FAUSTO STELLA, (Member, IEEE), AND GIANMARIO PELLEGRINO, (Fellow, IEEE)
Department of Energy "Galileo Ferraris," Politecnico di Torino, 10129 Torino, Italy

Corresponding author: Paolo Pescetto (paolo.pescetto@polito.it)

ABSTRACT The rapid spread of electric vehicles is pushing for more and more compact and reliable e-axle architectures. In this scenario, the integration of the on-board battery charger with the traction drive can be a feasible way to reduce the embedded volume and number of components. Anyway, integrated chargers often present safety issues due to the absence of an isolation stage. In this work, a solution is proposed for integrating the on-board battery charger with the traction drive of road electric vehicles equipped with a 6-phase traction motor drive. The proposed charger is deeply integrated within the e-drive powertrain, to reduce the cost and volume of the e-axle with respect to non-integrated solutions, but still providing galvanic insulation, differently from all fully integrated charger in the literature. Dedicated control strategies are developed and tested for regulating the AC grid current at unitary power factor and low THD, and to avoid torque production or rotor movement during charging independently from the rotor position. Extensive simulation results show the feasibility of the proposed solution, together with a proof-of-concept validation on a commercial traction motor.

I. INTRODUCTION

Electric Vehicles (EVs) sales are exponentially growing in the last years [1] in every class of vehicle, from urban mobility to long range vehicles. This trend is explained by a favorable legislation and by the related environmental benefits, but it imposes relevant technology challenges, thus pushing the academic and industrial research toward innovative solutions. Among the main R&D areas, advanced motor and power converters design are key to permit increasing the power density and reliability of the electrical architecture.

The traction motors adopted in automotive are traditionally 3-phase Permanent Magnet Synchronous Machines (PMSMs) or Induction Motors (IM), with the former ones often preferred for their higher efficiency and power density.

The associate editor coordinating the review of this manuscript and approving it for publication was Qinfen Lu.

Anyway, multi-three phase drives, traditionally adopted for high power wind turbines and ship propulsion [2], are progressively becoming appealing also in automotive sector [3], permitting a reduced phase current rating and a higher system reliability. Torque ripple mitigation, higher number of degrees of freedom for the control and better thermal management are also additional benefits. In particular, the adoption of 6-phase motors appears to be the best trade-off between the benefits of multi-three phase machines and the increased system complexity, permitting a relatively easy transition from the traditional 3-phase drives [4].

Another key technology to enable a wide diffusion of EVs is the availability of reliable and efficient charging solutions. With this respect, the two main research areas are related to fast-charging stations [5] and On-board Battery Chargers (OBC) [6]. If the fast-charging stations can reach up to 350 kW, thus providing a relevant range extension in a small

charging time, their diffusion is still limited. On the other hand, OBC converters are present in every electric vehicle, permitting overnight charge at low (3-6 kW) to medium (10-20 kW) power [7].

Two main families of OBCs are found in literature and industry: the stand-alone and the integrated chargers [7]. If the former consists of a dedicated power electronic converter adopted for battery charging only, the latter exploits the EV motor as inductive element and the traction inverter for regulating the energy conversion at charging stage. Integrated On-Board Chargers (IOBCs) pursue higher compactness of the e-axle and higher reliability, thanks to the lower number of converters. Moreover, the current rating of the traction drive can permit a higher charging power [8], [9] respect to the stand-alone counterparts. Anyway, most of the integrated OBC in the literature [8], [10], [11], [12], [13] and automotive industry [9] are designed for 3-phase motors and are not compatible with multi-three phase machines. Moreover, most of carmakers require an isolation stage galvanically separating the grid from the battery, but this is not provided by most of the integrated chargers [7], [14], [15], [16]. Additionally, some of the solutions proposed in the literature produce torque at the shaft during charging, which may cause vibration and need for rotor locking. Solutions as [8] even require free-shaft continuous rotation of the rotor during charging at grid electrical frequency, thus complicating the mechanical arrangement and introducing relevant friction and ventilation losses during charging. Finally, the solutions presented in [9], [11], and [10] are unidirectional, thus not permitting V2G operation.

The adoption of multi-three phase machines open a wider number of degrees of freedom for the drive reconfiguration [14], [15], [17], [18], thus opening the possibility of different IOBC topologies and control strategies. Still, topologies like [14] suppose the connection with an external isolation transformer, which is not always available especially for domestic charging, being the on-board architecture not isolated. Galvanic isolation without motor torque or movement is achieved in [17] and [18] for 6-phase drives, in the topologies called Isolated Fully Integrated (IFI) and Isolated Semi Integrated (ISI) chargers. The main drawback of [17] is that the motor phases to be connected to the grid are selected based on the rotor position. Moreover, the star points of the two 3-phase sets need to be accessible to permit the disconnection of one of the phases. Both these aspect imposes a complicated mechanical arrangement. The solution in [18] requires a considerably simpler reconfiguration, but still needs the addition of grid line inductors and a passive diode bridge.

In this work, the IFI-OBC concept is modified and improved by a novel control strategy, which drastically reduces the complexity of the mechanical reconfiguration. This control strategy also requires a dedicated transformation matrix for defining the inverter reference voltage. In this way, an innovative and feasible isolated IOBC is achieved.
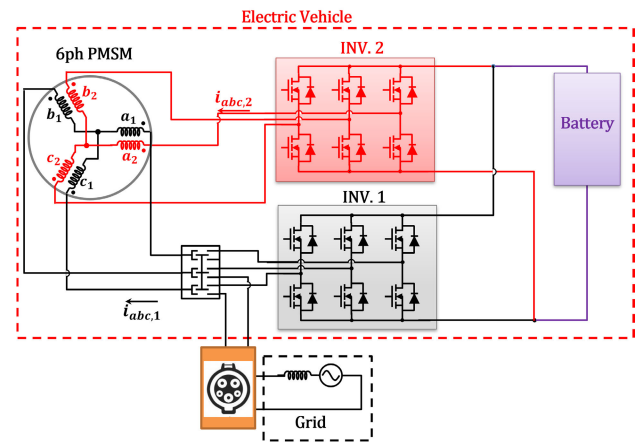

FIGURE 1. Six-phase traction e-drive, including the motoring/charging reconfiguration selector and the OBC grid connection.

TABLE 1. Ratings of the traction drive [26].

motor		
max power	120	kW
max torque	320	Nm
max speed	12000	rpm
pole pairs	3	

inverter		
max phase current	235	Arms
DC voltage	400	V
switching frequency	12÷50	kHz

The proposed IOBC permits an accurate control of the grid current quality and the absence of motor torque during charging. Finally, differently from many other topologies, the proposed OBC is bidirectional, thus permitting Vehicle to Grid (V2G) operation. The proposal is validated by accurate simulation models and by experimental tests on a proof-of-concept test rig employing a commercial 96 kW traction motor.

II. EV UNDER TEST AND IOBC SPECIFICATIONS

As mentioned, the EV under test [4] is equipped with a dual-three phase traction motor drive, as depicted in Figure 1. Table 1 reports the main motor and inverter ratings. The drive presents an anisotropic PMSM equipped with NdFeB permanent magnets and presenting two symmetric three-phase sets of stator windings [19], [20], indicated with the subscripts 1 and 2. Each winding set is fed by a 2-level 3-phase inverter module, called INV.1 and INV.2, integrated in the same inverter housing.

The specifications of the designed IOBC are defined based on the EV in [4] and on the present standards [21]:

- the IOBC should be realized with limited additional hardware respect to the drive itself
- galvanic isolation must be provided between the battery and the power grid

- the IOBC control must be capable of charging the battery either in Constant Voltage (CV) or Constant Current (CC) modes with a maximum power of 6.6 kW
- the grid current quality must fulfill the harmonic limits imposed by [21], with a PF>0.9
- no shaft torque, rotor movement or thermal stress of the motor must be produced during charging
- the charger must be bidirectional to ensure V2G capability.

As for any integrated battery chargers, the electric motor and inverter are adopted not only during traction, but also at battery charging stage. This requires a partial reconfiguration of the drive when switching between traction and charging modes. In addition to the above-mentioned requirements, the standards [22] and [23] impose, for the European and Chinese market respectively, that the voltage on the inlet connector of the EV must be below 30 Vrms when the EV is not plugged. Therefore, the reconfiguration must also guarantee the disconnection of the grid inlet terminals in traction mode. For this reason, as can be seen in Figure 1, a selector is added with respect to a standard 6-phase traction drive, to permit the EV reconfiguration from traction to charging mode, and vice versa. In particular, the selector connects the motor phases a_1, b_1, c_1 to the inverter in traction mode, or the phases b_1 and c_1 to the grid inlet in charging mode. No dynamic capabilities are required to such connector, as it only commutates at zero current when passing from traction to charging mode or vice-versa. Therefore, the selector can be optimized for reducing the conduction losses, regardless of the switching losses. Based on these considerations, the nature of the selector should be agreed upon with the carmaker. As an example, the selector can be an electronic switch, an electro-mechanical relay or a mechanical switch, and the three phases can either be integrated in a single selector or not.

III. MODELING OF THE DUAL 3-PHASE PMSM

A simple model of the dual-three phase PMSM is reported, introducing the key equations and notations. Space vector quantities are indicated in bold. The subscripts 1 and 2 refer to the first and second 3-phase set, while if the subscript number is missing the quantity refers to the magnetizing component. As for most of PMSMs, the d axis is oriented along the direction of PM magnetization, i.e. the minimum differential inductance direction.

The voltage in each 3-phase set $v_{dq,1}$ and $v_{dq,2}$ in dq reference frame is given by:

$$v_{dq,1} = R_s i_{dq,1} + \frac{d\lambda_{dq,1}}{dt} + J\omega\lambda_{dq,1} \quad (1)$$

$$v_{dq,2} = R_s i_{dq,2} + \frac{d\lambda_{dq,2}}{dt} + J\omega\lambda_{dq,2} \quad (2)$$

being R_s is the stator resistance, ω is the electrical angular frequency and $J = \begin{bmatrix} 0 & -1 \\ 1 & 0 \end{bmatrix}$ is the complex operator matrix. Considering the magnetic coupling of the two 3-phase set and the magnetic saturation effects, the flux linkage in each
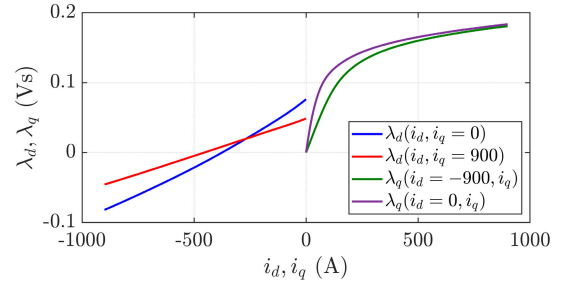

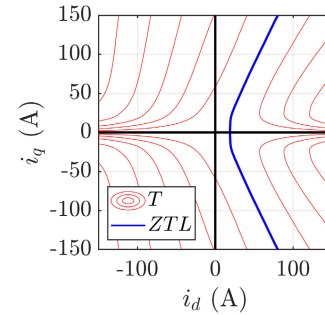**FIGURE 2. Saturation flux maps of the motor under test.**

FIGURE 3. Red: torque contour in the *dq* plane of the machine under test. Blue: zero torque locus.

3-phase set non-linearly depends on each of the 6 phase currents:

$$\begin{cases} \lambda_{dq,1} = \lambda_{dq,1}\left(i_{dq,1}, i_{dq,2}\right) \\ \lambda_{dq,2} = \lambda_{dq,2}\left(i_{dq,1}, i_{dq,2}\right) \end{cases} \quad (3)$$

The magnetizing current i_{dq} is defined as:

$$i_{dq} = i_{dq,1} + i_{dq,2} \quad (4)$$

The dual-three phase PMSM can be modeled as an equivalent transformer, where the flux linkage in each 3-phase set is given by a magnetizing component plus a leakage flux:

$$\lambda_{dq,1} = \lambda_{dq} + L_\sigma i_{dq,1} \quad (5)$$

$$\lambda_{dq,2} = \lambda_{dq} + L_\sigma i_{dq,2} \quad (6)$$

being L_σ is the leakage inductance. The magnetizing flux is derived from the common mode flux and current:

$$\lambda_{dq} = \frac{\lambda_{dq,1} + \lambda_{dq,2}}{2} - L_\sigma \frac{i_{dq,1} + i_{dq,2}}{2} \quad (7)$$

Because of magnetic saturation, the relationship between i_{dq} and λ_{dq} is nonlinear and specific for every motor. For the adopted PMSM, the flux maps, i.e. the nonlinear current-to-flux relationship considering magnetic saturation, are reported in Figure 2. As for most of the EV traction motors, the adopted PMSM is designed for high base and maximum speed, so the machine inductance is pretty low, in the order of magnitude of a few mH.

The motor torque can be computed as:

$$T = \frac{3}{2}p\left(\lambda_d i_q - \lambda_q i_d\right) \quad (8)$$

Since the machine under test is an anisotropic PMSM, the torque is a combination of PM and reluctance torque. These two components have opposite sign for $i_d > 0$, and a specific trajectory, called Zero Torque Locus (ZTL) [24], can be identified crossing the first and fourth quadrant of the dq plane where their effect is equal and opposite. If the magnetizing current vector i_{dq} lies on such trajectory, the developed shaft torque is null, as the PM and reluctance torque components are equal and opposite. For each point of the ZTL:

$$\lambda_d i_q = \lambda_q i_d \tag{9}$$

Fig. 3 shows the torque contour of the machine under test, with the ZTL highlighted in blue. The intercept between the ZTL and the d axis is called i_{dT0} [24]. This control law will be used for imposing zero torque during battery charge operation.

IV. IFI-OBC OPERATING PRINCIPLE

The concept of the proposed Isolated Fully-Integrated On-board Battery Charger (IFI-OBC) is to use the 6-phase PMSM as an isolation transformer at grid frequency, while the inverter regulates the energy conversion. The electrical architecture is reported in Figure 4. Among the benefits of this solution, a good grid power quality is achieved with minimal additional hardware. The only additional component is the selector which can either be a power electronic switch or an electromechanical actuator according to the carmaker's requirements, as discussed in Section II. Torque or rotor movements are not produced. Moreover, the proposed integrated battery charger is bidirectional, so V2G operation is also possible. In turn, all the specifications detailed in Section II are fulfilled.

As can be seen in Figure 4, one of the two inverter units (INV.1 in the Figure) is disconnected and not used. The motor terminals b_1 and c_1 of the correspondent 3-phase set are then connected to the single-phase grid. The third phase, i.e. a_1, is open. On the second 3-phase set, the winding connections are not modified, and each phase is regularly connected to the INV.2.

Under this reconfiguration, the first 3-phase set can be exploited as the primary winding of an equivalent isolation transformer, with the grid imposing a pulsating excitation voltage through the b_1 and c_1 phases of the PMSM. Considering the full machine, such excitation voltage and the corresponding flux linkage are in $b - c$ direction, i.e. aligned with the β axis of the PMSM. Because of the magnetic coupling of the 6-phase PMSM (3), the magnetizing flux imposed by the grid is linked also to the second 3-phase set of the PMSM, which behaves as the secondary winding of the equivalent transformer.

The INV.2 is controlled with a double purpose. On one side, the INV.2 control regulates the grid current, to ensure its sinusoidal waveform and high PF, as detailed in Section IV-A. At the same time, the control must ensure that torque is not produced during charging. Three different solution for zero
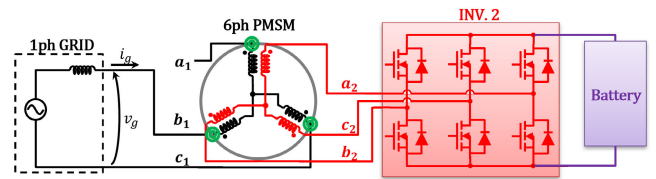

FIGURE 4. Proposed single-phase IFI-OBC topology.

torque control are proposed in Sections IV-B, IV-C and IV-D. The choice of the zero torque control technique depends on the EV architecture:

- if the e-axle presents a mechanical transmission with a disconnecting clutch, so that the PMSM can be mechanically disconnected from the wheels shaft at charging stage, the rotor will be aligned before starting the battery charging process, as described in Section IV-B;
- if the PMSM cannot be disconnected from the wheels, the adopted zero torque control depends on the rotor position θ, which is random when parking the car and must not be moved during charging. If $\theta \in \left(\frac{\pi}{4}, \frac{3\pi}{4}\right) \cup \left(\frac{5\pi}{4}, \frac{7\pi}{4}\right)$, the magnetizing current vector i_{dq} will be forced on the d axis, as detailed in Section IV-C, while if $\theta \in \left(-\frac{\pi}{4}, \frac{\pi}{4}\right) \cup \left(\frac{3\pi}{4}, \frac{5\pi}{4}\right)$ the i_{dq} would be forced on the ZTL, as described in Section IV-C.

The control block diagram is reported in Figure 6, where the blue box depicts the grid current control and the green box the zero torque control. The flow chart for determining of the zero torque control method to be adopted is summarized in Figure 5.

The main drawback of IFI-OBC is that, as the primary winding of the equivalent transformer is directly connected to the grid, the amplitude of the magnetizing flux is rigidly determined by the grid voltage amplitude and frequency:

$$\lambda \approx \frac{\hat{v}_g}{2\pi f_g} \tag{10}$$

where v_g and f_g are the inlet grid voltage amplitude and frequency. Considering a phase voltage of 230 Vrms @ 50 Hz, the resulting peak flux amplitude is approximately 1 Vs, which is too high for the PMSM under test (see Figure 2). Therefore, the proposed IFI-OBC is applicable assuming the motor windings can be reconfigured to increase the number of turns during charging. If the number of turns is increased by a factor n, the magnetizing flux and current λ'_{dq} and i'_{dq} in the reconfigured machine will be:

$$\lambda'_{dq} = n \cdot \lambda_{dq} \quad i'_{dq} = \frac{1}{n} \cdot i_{dq} \tag{11}$$

Such reconfiguration can be obtained, as an example, by changing the connection of the pole pairs from parallel to series. Since the machine under test presents 3 pole pairs, in the following we will assume $n = 3$.
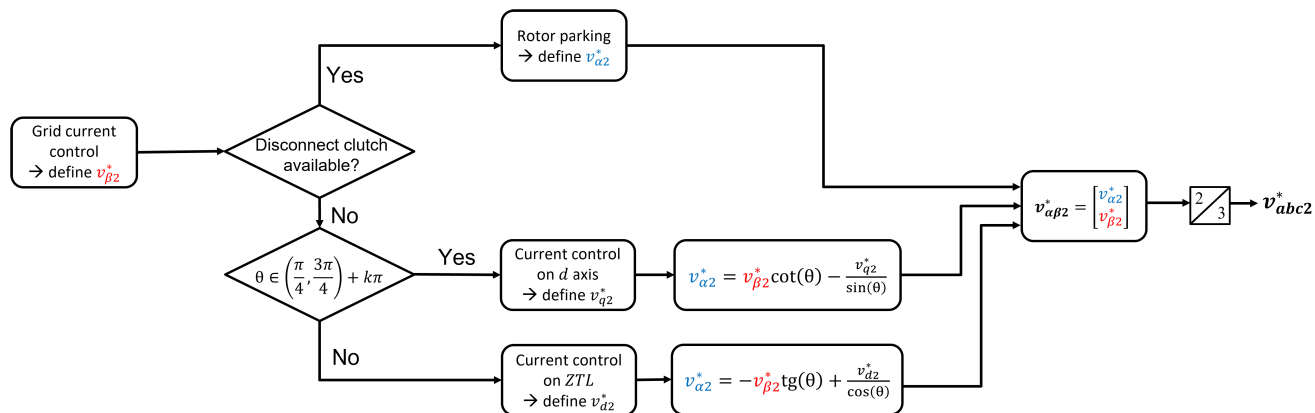
FIGURE 5. Flow chart for the selection of the zero torque control method.

A. GRID CURRENT CONTROL

As the grid terminals are connected to motor phases b_1 and c_1, the grid current is regulated through the voltage $v_{\beta2}$ of INV.2, which corresponds to the $b_2 - c_2$ direction. The control is performed through a non-conventional current loop, as shown in the blue box in Figure 6. The controlled variable is the grid current i_g, i.e. the current in the primary side of the equivalent transformer, flowing through the phases b_1 and c_1. The output of the regulator, enhanced by a feed-forward of v_g, is $v_{\beta2}$, i.e. the voltage imposed in the battery side.

It should be noted that a Proportional Resonant (PR) controller is required for proper current control, while a PI regulator, typically adopted for current control, cannot be adopted for two reasons. On one side, a PI regulator introduces a phase delay when controlling a sinusoidal current, unless it is calibrated with a considerably high bandwidth. Second, it should be noted that the voltage on the secondary side of the transformer is adopted to control the current in the primary side. This is feasible only for AC current components. If the system was controlled by a PI regulator, an eventual DC offset in the grid current measurement would result in an open loop integration from the integral branch of the PI, leading to the divergence of the control.

An external voltage loop sets the reference amplitude of i_g^* in order to obtain the desired voltage at the battery terminals. The reference v_{dc}^* is compared with the measured value v_{dc} and the discrepancy is input to a PI regulator, whose output is saturated at the maximum charging current amplitude. This permits to control the charging process either in CC (for low battery SOC) or CV (for high SOC) mode.

The phase of the grid voltage is extracted by a Phase Locked Loop (PLL) structure. The PLL type and dynamics are not deeply affecting the performance of the proposed OBC, so it will not be further discussed here. Several PLL present in the literature are suitable for a reliable grid phase estimation [25]. Based on the PLL bandwidth and nominal grid frequency, the introduced phase delay with respect to the grid angle $\Delta\varphi$ can be computed and feed-forward compensated.

B. ZERO TORQUE THROUGH ROTOR PARKING

Being the machine under test a PMSM, one solution to avoid torque is to align the rotor with the d axis along β direction ($\theta = \frac{\pi}{2}$), i.e. parallel to the flux generated by the grid excitation. In this way, the machine is naturally excited along the PM direction and no torque is produced. So, the INV.2 reference voltage $\mathbf{v}_{\alpha\beta2}^*$ can be determined as $v_{\alpha2} = 0$ and $v_{\beta2}$ defined by the grid current control, as per Section IV-A.

The rotor parking method permits accurate cancellation of the torque with a simple control, but it is feasible provided that the motor can be mechanically disconnected from the wheels shaft during charging stage. Considering that most of the modern EVs present a mechanical gearbox between the motor and the wheels shafts, the disconnection is possible if the transmission presents a disconnecting clutch. Otherwise, one of the methods described in Sections IV-C and IV-D must be adopted, still maintaining accurate zero torque control but slightly complicating the control scheme.

C. ACTIVE ZERO TORQUE CONTROL THROUGH D-AXIS CURRENT

In case the rotor cannot be mechanically disconnected from the e-axle, the torque an be actively controlled to be zero without moving the rotor from its initial position, which is random, and without necessarily locking it since no torque is produced. The active zero torque control strategy depends on the rotor position. This section describes the control feasible for $\frac{\pi}{4} < \theta < \frac{3\pi}{4}$ or $\frac{5\pi}{4} < \theta < \frac{7\pi}{4}$, which block diagram is reported in the green box of Figure 6(a). The zero torque control for a different rotor position is described in Section IV-D.

If the rotor position is within the indicated range, the β axis, i.e. the direction of grid excitation, is closer to the d axis with respect to the q axis, with a maximum displacement of
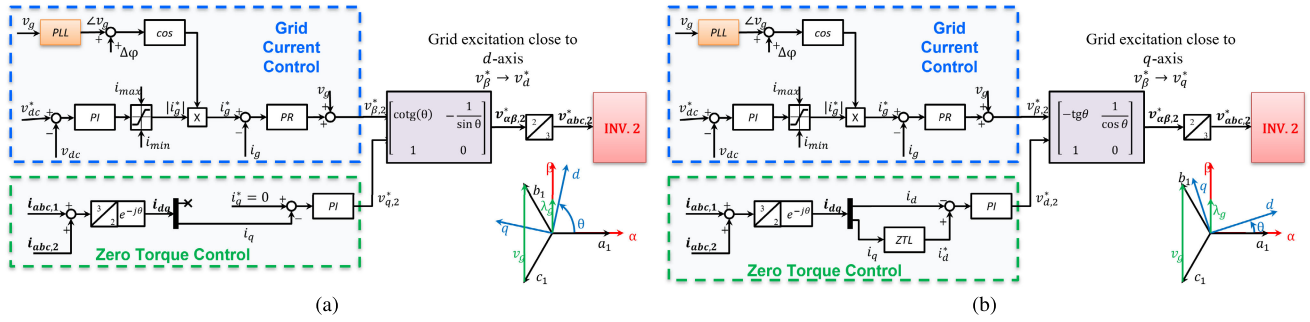
FIGURE 6. Control block diagram for the IFI-OBC. (a) Current control on *d* axis for $\frac{\pi}{4} < \theta < \frac{3\pi}{4}$. (b) Current control on the ZTL for $-\frac{\pi}{4} < \theta < \frac{\pi}{4}$.

$\frac{\pi}{4}$ between β and d directions. This means the machine will be mainly excited in d direction.

Considering (8), zero torque can eb obtained by forcing the magnetizing current vector i_{dq} to lay on the d axis. As can be seen in Figure 6(a), this is obtained by a second current control loop, forcing i_q to zero through a PI regulator. Note that if i_q is equal to zero, then also $\lambda_q = 0$ (see Figure 2), and so the torque is null. It should be noted that this is again a non-conventional current control: the magnetizing current component in q axis $i_q = i_{q1} + i_{q2}$ is controlled through the voltage on the secondary side only v_{q2}^*.

$$i_q = 0 \rightarrow T = 0 \qquad (12)$$

The voltage component v_{q2}^* adopted for zero torque control is combined with the voltage component $v_{\beta2}^*$, which regulates the grid current. This combination permits to obtain the reference voltage vector in $\alpha\beta$ frame:

$$\begin{bmatrix} v_{\alpha,2}^* \\ v_{\beta,2}^* \end{bmatrix} = \begin{bmatrix} \cot(\theta) & -\frac{1}{\sin(\theta)} \\ 1 & 0 \end{bmatrix} \begin{bmatrix} v_{\beta2}^* \\ v_{q2}^* \end{bmatrix} \qquad (13)$$

It should be noted that (13) merges two non-orthogonal voltage components. This is feasible provided that the angle between them is sufficiently large, as the equation diverges for $\theta \rightarrow 0 + k\pi$. Anyway, the condition $\theta \in \left(\frac{\pi}{4}, \frac{3\pi}{4}\right) \cup \left(\frac{5\pi}{4}, \frac{7\pi}{4}\right)$ ensures at least $\frac{\pi}{4}$ discrepancy between β and q directions, thus avoiding instability.

Finally, the inverse Clarke transformation is adopted to determine the reference voltage of INV.2 in abc frame v_{abc2}^*.

D. ACTIVE ZERO TORQUE CONTROL ON ZTL

If the rotor position falls in the range $-\frac{\pi}{4} < \theta < \frac{\pi}{4}$ or $-\frac{3\pi}{4} < \theta < \frac{5\pi}{4}$, the grid excitation is too far from the d axis, and forcing $i_q = 0$ would require a relatively high current in the secondary side of the equivalent transformer. Moreover, as mentioned above, if the β and q axes become too close, the two voltage components $v_{\beta2}^*$ and v_{q2}^* tend to collapse, leading (13) to diverge. Therefore, canceling the torque by forcing $i_q = 0$ is not possible.

As a feasible alternative, the magnetizing current vector i_{dq} is forced to lay on the ZTL, again implementing a non-conventional current control loop, according to the block
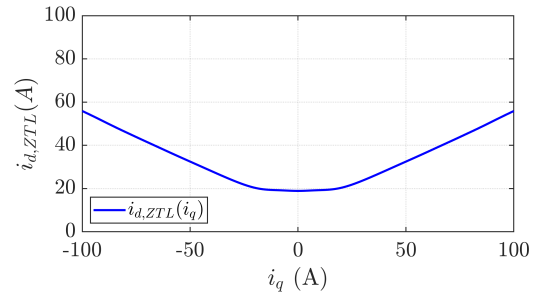

FIGURE 7. Selection of i_d^* based on the measured i_q.

diagram of Fig. 6(a). For doing so, the ZTL trajectory in the dq plane must be offline retrieved based on the machine flux maps, depicted in Fig. 2. In particular, the following function is needed:

$$i_{d,ZTL} = i_{d,ZTL}\left(i_q\right) \qquad (14)$$

where $i_{d,ZTL}$ is the value of i_d that meets the ZTL constrain for a given i_q. This function is graphically depicted in Fig. 7.

The magnetizing current vector i_{dq} is again computed from the measured phase currents in the two 3-phase sets (4). Because of the rotor position, the current in q axis is mostly determined by the grid voltage excitation and grid current control loop. The resulting i_q is adopted in (14) for retrieving the reference value of i_d^* which would drive the vector i_{dq} on the ZTL. The magnetizing current i_d is driven to the $i_d^*(i_q)$ value through a PI regulator, whose output is v_{d2}^*. This is feasible considering that the ZTL trajectory is almost parallel to the q direction, but shifted by the term i_{dT0}.

Similarly to (13), the voltage component $v_{\beta2}^*$ determined from the grid current control (Section IV-A) must be merged with the v_{d2}^* value derived from the zero torque control:

$$\begin{bmatrix} v_{\alpha,2}^* \\ v_{\beta,2}^* \end{bmatrix} = \begin{bmatrix} -\tan(\theta) & \frac{1}{\cos(\theta)} \\ 1 & 0 \end{bmatrix} \begin{bmatrix} v_{\beta2}^* \\ v_{d2}^* \end{bmatrix} \qquad (15)$$

The reference voltage of INV.2 v_{abc2}^* is again obtained from the inverse Clarke transformation.
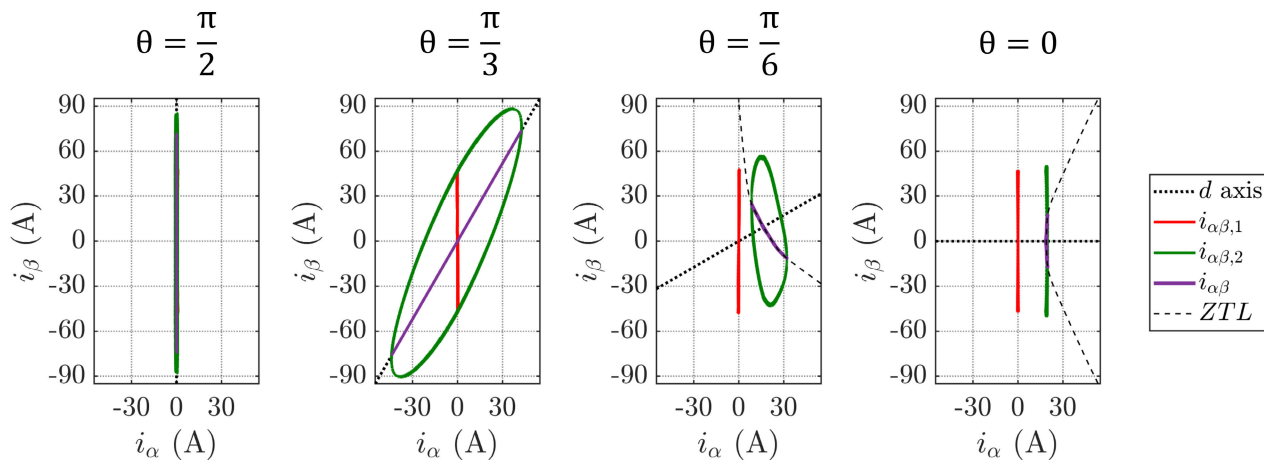
FIGURE 8. Trajectory of the current vectors on the $\alpha\beta$ plane for different rotor positions, as indicated on top of each plot. Blue: current on the primary side $i_{\alpha\beta 1}$. Red: current on the secondary side $i_{\alpha\beta 2}$. Green: magnetizing current $i_{\alpha\beta}$. The d axis and the ZTL are depicted as dotted and dashed black lines respectively.

V. SIMULATION RESULTS

The proposed IFI OBC of Figure 4 was validated by extensive simulations using PLECS software. As said, to avoid excessive core saturation in each test the number of turns is virtually increased by 3 times, assuming the winding configuration of the poles connections is changed from parallel to series.

The correct operation of the IFI-OBC was tested under different rotor positions, to test every proposed the zero torque control. At first, rotor parking is assumed, as described in Section IV-B. In this case, the rotor position is $\theta = \pi/2$, i.e. the d axis is aligned with β. The rated power 6.7 kW is absorbed from the grid. The results are depicted in Figure 9. The upper subplot shows the grid side voltage and current. Since the grid is connected between the phases b_1 and c_1, the grid voltage corresponds to $v_{bc,1}$ and the grid current is $i_g = i_b = -i_c$. The phase a is not connected, so $i_a = 0$. As can be seen, the current is properly controlled to be in phase with the grid voltage, with PF$\approx$1 and a THD$<$2.5%. Therefore, the grid constrains [21] are well respected.

The lower plot of the same Figure reports the corresponding voltage and current on the battery side of the PMSM, showing a similar voltage but a higher current and lower PF. This can be explained considering that the PMSM is acting as a transformer, so it has to absorb reactive power for magnetizing the rotor. Since PF $= 1$ on the primary side, such reactive power is given by the secondary side of the machine.

The two subplots of Figure 10 refer again to the current and voltage on the grid and battery side respectively, but in this case it is assumed that the EV does not present a disconnecting clutch, so the rotor parking is not possible, and the battery is charged with a rotor position $\theta = \pi/3$. Based on the flow chart in Figure 5, the torque is actively controlled to zero through the technique described in Section IV-C, i.e. by forcing the magnetizing current vector on the d axis. As can be noted, negligible discrepancy is observed in the
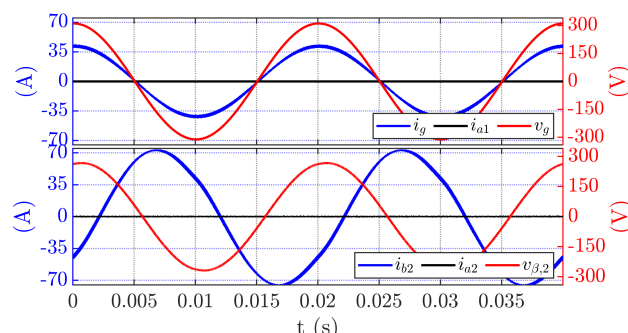

FIGURE 9. Results of IFI-OBC using initial parking ($\theta = \frac{\pi}{2}$). Upper plot: current and voltage on grid side of the PMSM. Lower plot: Current and voltage on the battery side.
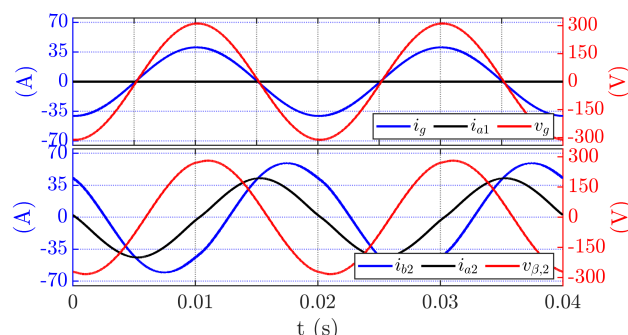

FIGURE 10. IFI-OBC using active zero torque control with magnetizing current on d axis for $\theta = \frac{\pi}{3}$. Upper plot: current and voltage on grid side of the PMSM. Lower plot: Current and voltage on the battery side.

grid current with respect to the parking case of Figure 9, as the adopted grid current control is the same (see Section IV-A), while in this case a current i_{a2} is present to drive i_q to zero.

Two further tests were performed for $\theta = \pi/6$ and $\theta = 0$, still at rated charging power. According to Figure 5, the torque is actively controlled to zero by forcing $\boldsymbol{i_{dq}}$ to lay on the
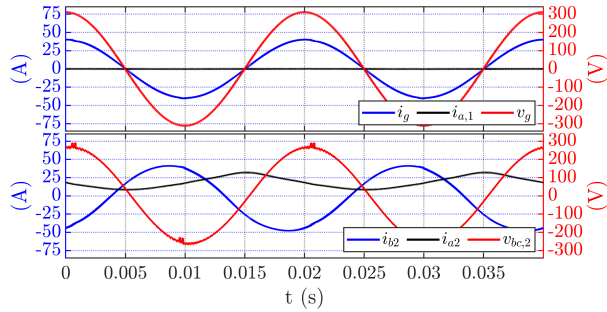
FIGURE 11. IFI-OBC using active zero torque control with magnetizing current on the ZTL for $\theta = \frac{\pi}{6}$. Upper plot: current and voltage on grid side of the PMSM. Lower plot: Current and voltage on the battery side.
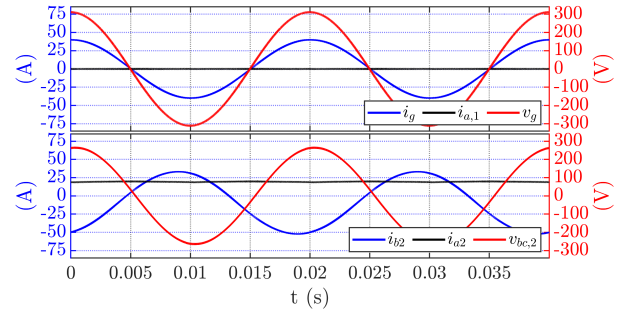

FIGURE 12. IFI-OBC using active zero torque control with magnetizing current on the ZTL for $\theta = 0$. Upper plot: current and voltage on grid side of the PMSM. Lower plot: Current and voltage on the battery side.

ZTL. The results are depicted in Figures 11 and 12 respectively. Also in these cases, the grid current quality is optimal, and with negligible discrepancy with respect to the previous simulations. In other words, the IFI-OBC is able to properly control the grid current regardless the method adopted for avoiding to produce torque, either free-shaft parking, active zero torque control on d axis or on the ZTL.

The subplots in Figure 8 show the trajectories of the current vectors $i_{\alpha\beta,1}$, $i_{\alpha\beta,2}$ and the magnetizing current $i_{\alpha\beta}$ in the $\alpha\beta$ plane for the four tested cases, i.e. $\theta = \pi/2$, $\theta = \pi/3$, $\theta = \pi/6$ and $\theta = 0$. For every subplot, being the a_1 phase disconnected, the current vector $i_{\alpha\beta,1}$ moves along β direction, while the trajectory of $i_{\alpha\beta,2}$ depends on the adopted zero torque technique. In the first subplot (rotor parking), $i_{\alpha\beta,2}$ is controlled on β, which corresponds to the d axis. Therefore, $i_{\alpha\beta}$ is again on $\beta = d$, i.e. aligned with the PM direction, and torque is not produced. In the second subplot, ($\theta = \pi/3$) the control imposes the magnetizing component i_q to be null, as in Figure 6(a). This results in the vector $i_{\alpha\beta}$ to lay again on d axis, depicted in dotted line, even if this is 30° shifted from β, and torque is again null. In the third and fourth subplots ($\theta = \pi/6$ and $\theta = 0$), the main excitation is still imposed by the grid in β direction, but the active zero torque control imposes a nonlinear current vector $i_{\alpha\beta,2}$ which deviates the magnetizing current, so that it instantaneously lays on the ZTL, reported with dashed line. In these cases, (9) holds and torque is again null. In the specific case of $\theta = 0$, the current vector $i_{\alpha\beta,2}$ results almost parallel to β, but shifted by the term i_{dT0}, defined in Section III.

Finally, Figure 13 shows the motor torque in the four tested cases. As can be noted, all the proposed techniques for torque cancellation work very well. The residual torque is lower than 0.5 Nm. If compared to the rated peak torque of 320 Nm, such residual torque can be considered negligible, and well in accordance with the mechanical specifications given by the carmaker. It should be remarked that without one of the proposed techniques, the shaft torque would be very high, comparable with the rated motor torque.

Overall, the IFI-OBC results are promising, demonstrating effective charging capability without torque production independently by the rotor position.
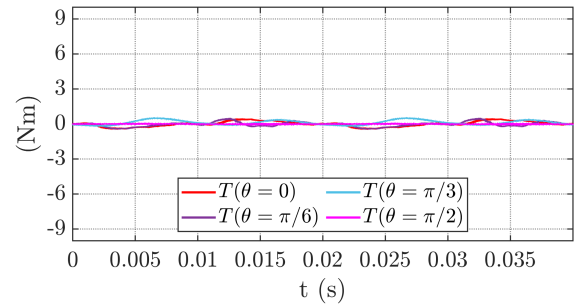

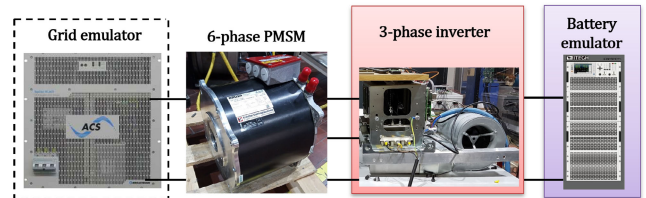**FIGURE 13.** Shaft torque obtained with the four simulated rotor positions.

FIGURE 14. Test bench for experimental validation of IFI-OBC.

VI. EXPERIMENTAL RESULTS

The proposed IFI-OBC has been tested on a full scale prototype of 6-phase machine for EV traction, based on the commercial motor in [26]. The test bench, including a grid emulator, the motor under test, the adopted inverter and a battery emulator, is depicted in Figure 14. It has been decided to perform the tests at free-shaft, which is the worst case scenario for demonstrating the zero torque production and the absence of rotor movement. Anyway, the free-shaft solution does not permit to externally impose the initial rotor position, so only the control method in Section IV-C was experimentally tested.

As declared in Section IV, the IFI-OBC is applicable provided that the number of turns of the machine can be increased, e.g. by changing the poles connection from parallel to series, to avoid core saturation. Since the adopted prototype does not have this feature, a similar effect on the magnetizing flux has been realized by reducing the grid voltage amplitude, synthesized by the grid emulator.
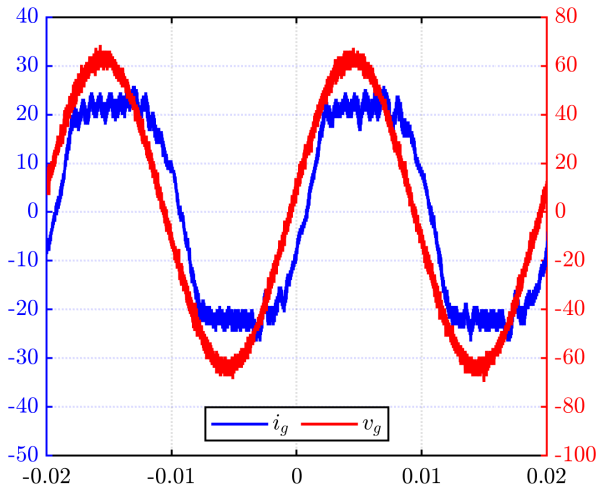
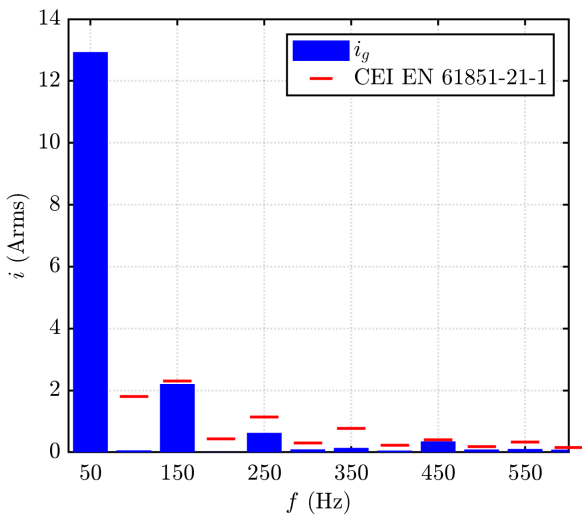**FIGURE 15.** Experimental: grid voltage (red) and current (blue).

FIGURE 16. Experimental: grid current harmonic content. The red lines represent the limits imposed by the standards [21].

FIGURE 17. Experimental: voltage (red) and current (blue) on the battery side, in *dq* coordinates.
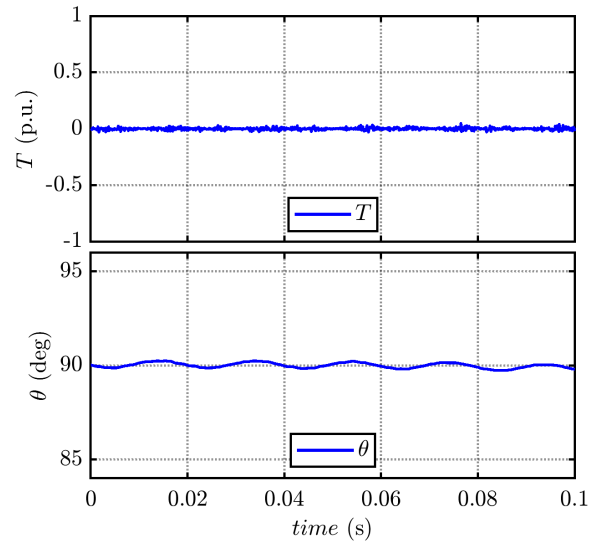
FIGURE 18. Experimental: motor torque and position.

The experimental grid voltage and current are depicted in Figure 15, where zero torque was obtained by forcing the current on d axis. As can be noted, the grid current presents a slight delay with respect to the grid voltage, but still maintaining a PF of 0.94, in line with the standards [21]. Dealing with the harmonic distortion, the harmonic content of the grid current is compared with the limits imposed by [21] in Figure 16, resulting again compliant with the standards.

It should be noted that the motor winding reconfiguration described in Section II, and not applicable in the available prototype, would also increase the leakage inductance by n^2 times, thus significantly reducing the grid current ripple with respect to the results shown in Figure 16.

For the same experimental test, Figure 17 depicts the voltage and current in the secondary side in dq coordinate, while the motor torque and position are reported in Figure 18.
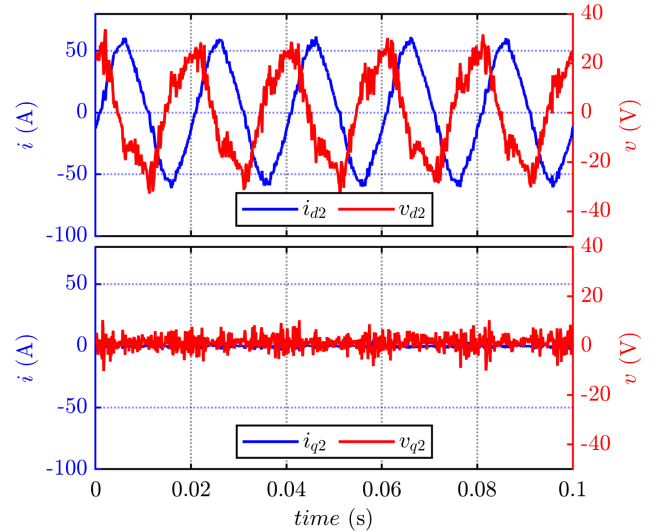
As can be noted, the proposed zero torque control is effective, correctly canceling the current in the q axis. Therefore, the developed torque is negligible, especially if compared with the motor torque during traction. The electrical rotor position is depicted in the lower plot of Figure 18, showing limited oscillations lower than 0.5°, corresponding to a negligible mechanical deviation. Considering that the test is run at free-shaft, i.e. the worst case mechanical scenario, this is a further confirmation of the correct torque cancellation.

The efficiency of the proof-of-concept demonstrator is highly affected by the adopted inverter, which is based on industrial IGBT power modules (see Figure 14) not designed for high efficiency. On the other side, a commercial traction PMSM was adopted, which is well representative of

a real-case scenario in automotive. Based on the current and voltage at the input and output of the machine, the losses in the equivalent transformer could be determined, estimating an efficiency of ≈93%.

VII. CONCLUSION

In this work, an isolated on-board battery charger has been developed and integrated with a traction motor drive based on a 6-phase PMSM. The proposed topology permits galvanic isolation between the grid and the battery by exploiting the traction motor as a transformer, without the addition of electrical hardware out of the drive itself except for a reconfiguration selector, which may be electrical or mechanical depending on the specifications of the carmaker. Dedicated control techniques have been developed for accurately controlling the grid current and avoid torque production during charging, as required by automotive specifications and standards. Different techniques are adopted based on the availability or not of a mechanical disconnecting clutch and on the initial rotor position, leading to similar performance. The proposal is supported by extensive simulation results and by experiments on a proof-of-concept IOBC based on a commercial traction motor.

REFERENCES

[1] IEA. *Global Electric Vehicle Outlook 2022*. Accessed: Oct. 2022. [Online]. Available: https://www.iea.org/reports/global-ev-outlook-2022

[2] E. Levi, "Multiphase electric machines for variable-speed applications," *IEEE Trans. Ind. Electron.*, vol. 55, no. 5, pp. 1893–1909, May 2008.

[3] A. Salem and M. Narimani, "A review on multiphase drives for automotive traction applications," *IEEE Trans. Transport. Electrific.*, vol. 5, no. 4, pp. 1329–1348, Dec. 2019.

[4] M. Martino, P. Pescetto, and G. Pellegrino, "Advanced functionally integrated e-axle for A-segment electric vehicles," in *Proc. AEIT Int. Conf. Electr. Electron. Technol. Automot. (AEIT AUTOMOTIVE)*, Nov. 2020, pp. 1–6.

[5] H. Tu, H. Feng, S. Srdic, and S. Lukic, "Extreme fast charging of electric vehicles: A technology overview," *IEEE Trans. Transport. Electrific.*, vol. 5, no. 4, pp. 861–878, Dec. 2019.

[6] A. Khaligh and S. Dusmez, "Comprehensive topological analysis of conductive and inductive charging solutions for plug-in electric vehicles," *IEEE Trans. Veh. Technol.*, vol. 61, no. 8, pp. 3475–3489, Oct. 2012.

[7] M. Yilmaz and P. T. Krein, "Review of battery charger topologies, charging power levels, and infrastructure for plug-in electric and hybrid vehicles," *IEEE Trans. Power Electron.*, vol. 28, no. 5, pp. 2151–2169, May 2013.

[8] S. Haghbin, K. Khan, S. Zhao, M. Alakula, S. Lundmark, and O. Carlson, "An integrated 20-kW motor drive and isolated battery charger for plug-in vehicles," *IEEE Trans. Power Electron.*, vol. 28, no. 8, pp. 4013–4029, Aug. 2013.

[9] S. Loudot, B. Briane, O. Ploix, and A. Villeneuve, "Fast charging device for an electric vehicle," U.S. Patent 2012 0 286 740 A1, Nov. 15, 2012.

[10] L. Solero, "Nonconventional on-board charger for electric vehicle propulsion batteries," *IEEE Trans. Veh. Technol.*, vol. 50, no. 1, pp. 144–149, Jan. 2001.

[11] G. Pellegrino, E. Armando, and P. Guglielmi, "An integral battery charger with power factor correction for electric scooter," *IEEE Trans. Power Electron.*, vol. 25, no. 3, pp. 751–759, Mar. 2010.

[12] A. Bruyère, L. De Sousa, B. Bouchez, P. Sandulescu, X. Kestelyn, and E. Semail, "A multiphase traction/fast-battery-charger drive for electric or plug-in hybrid vehicles: Solutions for control in traction mode," in *Proc. IEEE Vehicle Power Propuls. Conf.*, Lille, France, Sep. 2010, pp. 1–7.

[13] S. Lacroix, E. Laboure, and M. Hilairet, "An integrated fast battery charger for electric vehicle," in *Proc. IEEE Vehicle Power Propuls. Conf.*, Lille, France, Sep. 2010, pp. 1–6.

[14] I. Subotic, N. Bodo, and E. Levi, "Single-phase on-board integrated battery chargers for EVs based on multiphase machines," *IEEE Trans. Power Electron.*, vol. 31, no. 9, pp. 6511–6523, Sep. 2016.

[15] I. Subotic, N. Bodo, E. Levi, B. Dumnic, D. Milicevic, and V. Katic, "Overview of fast on-board integrated battery chargers for electric vehicles based on multiphase machines and power electronics," *IET Electr. Power Appl.*, vol. 10, no. 3, pp. 217–229, 2016.

[16] M. C. Kisacikoglu, M. Kesler, and L. M. Tolbert, "Single-phase on-board bidirectional PEV charger for V2G reactive power operation," *IEEE Trans. Smart Grid*, vol. 6, no. 2, pp. 767–775, Mar. 2015.

[17] P. Pescetto and G. Pellegrino, "Integrated isolated OBC for EVs with 6-phase traction motor drives," in *Proc. IEEE Energy Convers. Congr. Expo. (ECCE)*, Detroit, MI, USA, Oct. 2020, pp. 4112–4117.

[18] P. Pescetto and G. Pellegrino, "Isolated semi integrated on-board charger for EVs equipped with 6-phase traction drives," in *Proc. 47th Annu. Conf. IEEE Ind. Electron. Soc. (IECON)*, Toronto, ON, Canada, Oct. 2021.

[19] F. Barrero and M. J. Duran, "Recent advances in the design, modeling, and control of multiphase machines—Part I," *IEEE Trans. Ind. Electron.*, vol. 63, no. 1, pp. 449–458, Jan. 2016.

[20] P. Xu, J. H. Feng, S. Y. Guo, S. Feng, W. Chu, Y. Ren, and Z. Q. Zhu, "Analysis of dual three-phase permanent-magnet synchronous machines with different angle displacements," *IEEE Trans. Ind. Electron.*, vol. 65, no. 3, pp. 1941–1954, Mar. 2018.

[21] *IEC 61851-1:2017 Electric Vehicle Conductive Charging System*, International Standard IEC 61851-1:2017-02, 2017.

[22] *UNECE R100, Uniform Provisions Concerning the Approval of Vehicles With Regard to Specific Requirements for the Electric Power Train*. Accessed: Aug. 2013. [Online]. Available: https://unece.org/sites/default/files/2022-07/R100r3e.pdf

[23] *Electric Vehicles Safety Requirements*, Standard GB 18384-2020, 2020.

[24] P. Pescetto and G. Pellegrino, "Determination of PM flux linkage based on minimum saliency tracking for PM-SyR machines without rotor movement," *IEEE Trans. Ind. Appl.*, vol. 56, no. 5, pp. 4924–4933, Sep. 2020.

[25] R. Teodorescu, M. Liserre, and P. Rodriguez, "Grid synchronization in singlephase power converters," in *Grid Converters for Photovoltaic and Wind Power Systems*. Chichester, U.K.: Wiley, 2007, pp. 43–91.

[26] *Brusa Elektronik AG, HSM1.6.17.12*. Accessed: Oct. 2022. [Online]. Available: https://www.brusa.biz/portfolio/hsm1-6-17-12-2/

PAOLO PESCETTO (Member, IEEE) received the B.Sc. and M.Sc. degrees (Hons.) and the Ph.D. degree (cum laude) from Politecnico di Torino, Turin, Italy, in 2013, 2015, and 2019, respectively. Since Fall 2019, he has been a Researcher and a tenure track Lecturer with the Energy Department, Politecnico di Torino, where he is a member of the Power Electronics Innovation Center (PEIC). In 2014, he was an Erasmus Student with the Norwegian University of Science and Technology, Trondheim. He has authored or coauthored more than ten IEEE journal articles. His main research interests include synchronous motor drives, sensorless control, self-commissioning techniques, and integrated battery chargers for EVs. He received five IEEE paper awards and two IEEE Ph.D. thesis awards.

MATIAS FERNANDO TRONCOSO CRUZ (Member, IEEE) was born in Chile, in 1988. He received the M.Sc. degree in electrical engineering from Politecnico di Torino, Turin, Italy, in 2013, and the double degree from Pontificia Universidad Catolica de Chile (PUC), Chile. He is currently pursuing the industrial Ph.D. degree with the Power Electronics Interdepartmental Laboratory (PEIC), Politecnico di Torino, for an automotive company in Italy. He received a professional title in industrial engineering with a focus on electrical engineering from PUC, in 2013. He was with Coener, where he worked in the field of renewable energies. He performed laboratory courses in PUC and co-founded the startups RT Electronics and Reborn Electric in Chile. He is working with an automotive company, Italy, in the field of testing components for hybrid vehicle applications.

FAUSTO STELLA (Member, IEEE) received the bachelor's and master's degrees in electrical engineering and the Ph.D. degree from Politecnico di Torino, Turin, Italy, in 2012, 2015, and 2019, respectively. In 2017, he was a Visiting Ph.D. Student with the University of Nottingham, U.K. He is currently an Assistant Professor with Politecnico di Torino, where he is also a Research Fellow. His research interests include the design of power electronic converters, focusing on SiC semiconductors and reliability issues, and the control of converters via embedded systems.

GIANMARIO PELLEGRINO (Fellow, IEEE) received the M.Sc. and Ph.D. degrees in electrical engineering from Politecnico di Torino, Turin, Italy, in 1998 and 2002, respectively. He is a Full Professor of power converters, and electrical machines and drives with Politecnico di Torino. He was a Visiting Scholar with Aalborg University, Denmark, in 2002; the University of Nottingham, U.K., from 2010 to 2011; and the University of Wisconsin–Madison, USA, in 2013. He is engaged in several funded and commercial research projects in the fields of electric motor design and e-drives control. He is a founding author of the open-source project SyR-e for the design of electrical motors and drives. He has coauthored 190 Scopus-indexed technical publications, including 60 IEEE journal articles, two books, and eight patents. He is a Founding Member of the Power Electronics Interdepartmental Center (PEIC), Politecnico di Torino, a member of the Advisory Board of PCIM Europe, and the Advisor to the Rector of Politecnico di Torino for the implementation of interdepartmental centers of Politecnico di Torino. He was a recipient of the eighth Grand Nagamori Award and nine best paper awards. He is an Associate Editor of the IEEE Transactions on Industry Applications.

• • •